JOURNAL OF SPACECRAFT AND ROCKETS
Vol. 46, No. 5, September–October 2009

Survey of Supersonic Retropropulsion Technology for Mars Entry, Descent, and Landing

Ashley M. Korzun* and Robert D. Braun†
Georgia Institute of Technology, Atlanta, Georgia 30332-0150
and
Juan R. Cruz‡
NASA Langley Research Center, Hampton, Virginia 23681-2199

DOI: 10.2514/1.41161

Nomenclature

A	=	area, m^2
C	=	force coefficient
M	=	Mach number
m	=	mass, kg
P	=	pressure, Pa
q	=	dynamic pressure, Pa
T	=	thrust, N
W	=	weight, N
α	=	angle of attack, deg
β	=	vehicle ballistic coefficient, kg/m^2

Subscripts

A	=	axial force
B	=	vehicle or model base
D	=	drag
e	=	nozzle exit
M	=	moment
prop	=	propellant
T	=	thrust
∞	=	freestream condition

Ashley M. Korzun received her B.S. in aerospace engineering from the University of Maryland, College Park, and her M.S. in aerospace engineering from the Georgia Institute of Technology. She is currently pursuing a Ph.D. as a graduate research assistant in aerospace engineering at the Georgia Institute of Technology in the Space Systems Design Laboratory. Her research focuses on supersonic retropropulsion for planetary entry, descent, and landing applications, specifically for Mars, including systems-level analysis and the development of computational fluid dynamics approaches for modeling aerodynamics and aerothermodynamics. She is currently a Student Member of AIAA.

Robert D. Braun is the David and Andrew Lewis Associate Professor of Space Technology in the Guggenheim School of Aerospace Engineering at the Georgia Institute of Technology. As Director of the Georgia Institute of Technology's Space Systems Design Laboratory, he leads a research program focused on the design of advanced flight systems and technologies for planetary exploration. Before coming to the Georgia Institute of Technology, he served on the technical staff of the NASA Langley Research Center for sixteen years, where he worked extensively in the areas of entry system design, planetary atmospheric flight, and mission architecture development. He is an AIAA Fellow and the principal author or coauthor of over 100 technical publications in the fields of planetary exploration, atmospheric entry, multidisciplinary design optimization, and systems engineering. He has a B.S. in aerospace engineering from Pennsylvania State University, an M.S. in astronautics from George Washington University, and a Ph.D. in aeronautics and astronautics from Stanford University.

Juan R. Cruz is an aerospace engineer in the Atmospheric Flight and Entry Systems Branch of the NASA Langley Research Center. He has been involved with the development and qualification of the entry, descent, and landing system of several planetary exploration missions, including the Mars Exploration Rovers and the Mars Science Laboratory. His current research focuses on the development of aerodynamic decelerators for planetary exploration missions. He has an S.B. in aeronautics and astronautics from the Massachusetts Institute of Technology, an M.S. in aerospace engineering from George Washington University, and a Ph.D. in aerospace engineering from Virginia Polytechnic Institute and State University.

Presented at the IEEE Aerospace Conference, Big Sky, MT, 1–8 March 2008; received 22 September 2008; accepted for publication 1 July 2009. Copyright © 2009 by the American Institute of Aeronautics and Astronautics, Inc. The U.S. Government has a royalty-free license to exercise all rights under the copyright claimed herein for Governmental purposes. All other rights are reserved by the copyright owner. Copies of this paper may be made for personal or internal use, on condition that the copier pay the $10.00 per-copy fee to the Copyright Clearance Center, Inc., 222 Rosewood Drive, Danvers, MA 01923; include the code 0022-4650/09 and $10.00 in correspondence with the CCC.

*Graduate Research Assistant, Guggenheim School of Aerospace Engineering. Student Member AIAA.
†Associate Professor, Guggenheim School of Aerospace Engineering. AIAA Fellow.
‡Aerospace Engineer, Atmospheric Flight and Entry Systems Branch.

I. Introduction

TO DATE, the United States has successfully landed six robotic missions on Mars: Viking 1 and 2, Mars Pathfinder, two Mars Exploration Rovers, and Phoenix. Including missions launched by the end of the decade, the largest entry mass sent to Mars will be the 2011 Mars Science Laboratory at ∼3250 kg. The entry, descent, and landing (EDL) systems for these missions rely heavily on extensions of Viking-heritage technology, namely, supersonic disk-gap-band (DGB) parachutes, 70 deg sphere–cone aeroshells, and subsonic propulsive terminal descent [1]. At Mars, aeroshell size constraints, high entry ballistic coefficients, and insufficient atmospheric density often result in unacceptable parachute deployment and operating conditions. An alternative deceleration approach is to initiate a retropropulsion phase while the vehicle is traveling at supersonic speeds. Supersonic retropropulsion may be an enabling decelerator technology for high-mass systems operating in thin atmospheres, such as Mars's.

A focused technology program preceding the Viking missions in the 1960s and 1970s developed supersonic retropropulsion to nearly the level of maturity the concept has today. The eventual selection of a supersonic DGB parachute system and subsonic propulsive terminal descent phase for the Viking landers ended much of the research efforts to develop supersonic retropropulsion. Only recently has interest in supersonic retropropulsion resurfaced. The applicability of Viking EDL technologies to the high-mass planetary entries needed for human Mars exploration has been shown to be constrained by deployment conditions and the performance of supersonic DGB parachutes [1]. These physical constraints have led to the recommendation to develop alternative supersonic decelerators.

Investigation into the interaction of retropropulsion with supersonic aerodynamics began in the early 1950s. Experimental work with small-scale wind-tunnel models by Love [2,3], Love et al. [4], Huff and Abdalla [5], and Moeckel [6,7] focused on shock–boundary-layer phenomena and the effects of retropropulsion nozzle flow on boundary-layer transition. These investigations were among the earliest observations of aerodynamic-propulsive interactions for retropropulsion configurations with a nozzle aligned with the body centerline. They are consistent in observing that increasing thrust coefficient [C_T defined in Eq. (1)] decreases aerodynamic drag and moves the boundary-layer transition closer to the nose of the body [2–7]. The thrust coefficient is a force coefficient, defined as the ratio of the thrust, T, to the freestream dynamic pressure, q_∞, and the vehicle base area, A_B:

$$C_T = T/(q_\infty A_B) \tag{1}$$

Additional work [4,5,8,9] on supersonic jet flow and jet–body interactions established the groundwork for future wind-tunnel testing of the effects of supersonic nozzle exhaust on surface pressure distributions and flowfield stability. Although many of these early body geometries were not the blunted-cone entry vehicle shapes flown in the 1960s and 1970s, these works outlined the fundamental physics of jet–shock interactions and motivated later investigations to apply such interaction effects to blunt body entry vehicles for planetary exploration.

This early retropropulsion work was extended to blunt body entry geometries in the 1960s and early 1970s, primarily through wind-tunnel experiments with small-scale models. Among the concepts investigated were single- and multiple-nozzle configurations, with the retropropulsion nozzles placed at either the center or the periphery of the vehicle forebody. Experimental results for low thrust coefficients consistently show significant increases in the total axial force coefficient (summation of aerodynamic drag and thrust coefficients) for the peripheral nozzle locations [10–12]. For high thrust coefficients, all nozzle configurations contributed substantially to the effective total axial force coefficient, though by thrust coefficient contributions only (little or no aerodynamic drag coefficient contribution) [10,12–18]. Additionally, the stability of the flowfield and resulting aerodynamic effects were found to be strongly dependent on the ratio of the jet total pressure to the freestream total pressure [10–26].

Although the majority of the literature is concentrated on decelerator applications of supersonic retropropulsion, potential aerothermal effects, test scaling parameters, and the capabilities of modern computational analysis have also been explored [10,15,19,21–32]. Both the experimental and computational work show the aerothermal effects of retropropulsion to be important, with the potential for doubling the local heat transfer to the body when combustion products are injected into the shock layer [15,19,21–29]. Experimental work has produced relationships for scaling and developed the primary similarity parameters for model and nozzle design. Computational investigations are ongoing, and early code validation efforts show good agreement with existing experimental data for axisymmetric configurations.

This paper provides a survey of the literature on the effects of retropropulsion on blunt body entry vehicles in an opposing supersonic freestream. The focus is on aerodynamic performance effects for application to EDL design and computational simulation development. This paper does not discuss nonpropulsive supersonic decelerators, reaction control system interactions, detailed aerothermodynamic issues, slender body geometries, or exhaust plumes in directions other than directly opposite the freestream. Section II discusses retropropulsion performance in Mars EDL systems. Sections III and IV compare results for central and peripheral nozzle configurations, as well as the effects of variations in environment and design parameters such as nozzle geometry and chemical composition of the freestream and retropropulsion exhaust. A summary of the existing experimental database is also provided. Section V discusses the computational simulation of supersonic retropropulsion flowfields and the extensibility and limitations of this work.

II. Retropropulsion System Performance

Human Mars architecture studies predict payload masses on the order of 20–100 t [33–35]. The EDL requirements of these high-mass, high-ballistic-coefficient [β defined in Eq. (2)] systems extend well beyond the capabilities of many Viking-heritage EDL technologies, with supersonic deceleration as possibly the most critical deficiency. The high ballistic coefficients in these architecture studies (∼300 kg/m^2 and higher), the thin atmosphere, and the inability to increase supersonic DGB parachutes to the required dimensions and deployment conditions severely reduce the timeline available for deceleration and the transition from a hypersonic entry vehicle to a terminal landing (subsonic) configuration [1].

$$\beta = m/(C_D A) \tag{2}$$

The point design in NASA's 1998 Mars Design Reference Mission [33,34] attempted to address the supersonic deceleration gap by using a cluster of 50-m-diam supersonic parachutes, followed by a subsonic propulsive terminal descent. Alternatively, Christian et al. [35] replaced the traditional parachute system with a purely propulsive descent initiated at supersonic conditions. Because these studies were for human class missions, with payload masses ranging from 20 to 100 t, significantly larger propulsion systems were required than had been flown previously. In these studies [33–37], the descent propulsion systems for supersonic deceleration were assumed to be liquid-oxygen/methane RD-180 derivatives, with an engine thrust to weight ratio (T/W) of 80 and a maximum thrust of 1 MN.

Among previous Mars EDL architectural studies in the literature, only the investigations by Christian et al. [35] and Wells et al. [36] initiated retropropulsion at supersonic conditions. In these two studies, the aerodynamic interactions of supersonic retropropulsion were not modeled (i.e., the deceleration was assumed to be provided solely by thrust). Past experimental evidence suggests that, for configurations with the nozzles located at the forebody periphery, inclusion of aerodynamic interaction effects into supersonic retropropulsion performance models will improve the fidelity of the vehicle aerodynamics model, reducing the propellant mass required for conditions preserving a portion or even all of the aerodynamic drag. In particular, for a retropropulsion configuration in which the

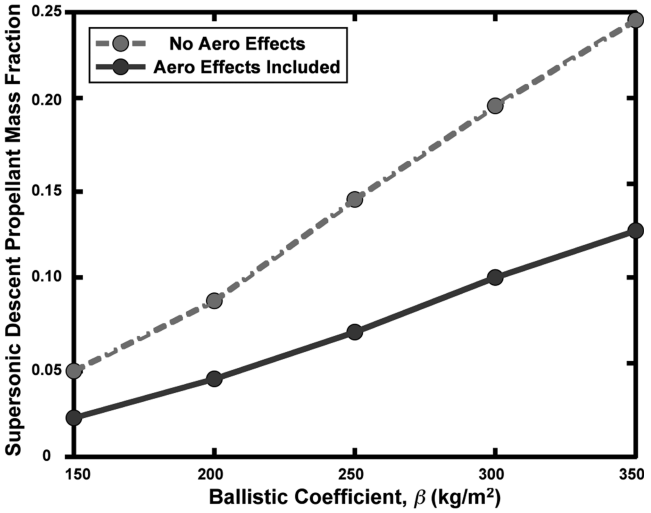

Fig. 1 Impact of neglecting aerodynamic-propulsive interactions during supersonic deceleration on descent propellant mass fraction for a configuration with nozzles located at the vehicle periphery ($C_T = 1.0$).

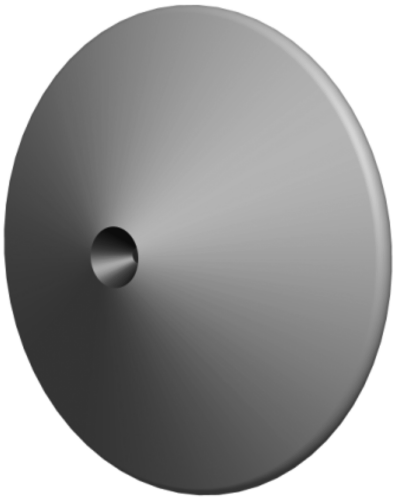

Fig. 2 Example of a central retropropulsion configuration with a single nozzle.

nozzles are located on the forebody periphery, the maximum thrust coefficient for full preservation of the aerodynamic drag coefficient is $C_T \sim 1$, with at least partial C_D preservation up to $C_T \sim 3$ [10]. Hence, proper modeling of the supersonic retropropulsion system can have a dramatic impact on EDL architectural performance in cases in which the required thrust coefficient is less than approximately 3.

For this literature review, a brief study was conducted to develop a general relationship between the required descent propellant mass fraction and vehicle ballistic coefficient. This relationship is shown in Fig. 1. The descent propellant mass fraction (PMF) is defined as the propellant mass required to decelerate the vehicle from supersonic retropropulsion initiation to subsonic conditions divided by the vehicle entry mass. This figure illustrates the increasing benefit of a properly designed supersonic retropropulsion system on the required descent propellant mass fraction as ballistic coefficient increases for a 15-m-diam Apollo aeroshell and $C_T = 1.0$. The data presented are for the minimum retropropulsion initiation Mach number to reach subsonic conditions at 3 km altitude in each case. Assuming a gravity turn subsonic descent trajectory results in a PMF of ~0.15, the difference between the total descent PMF (supersonic + subsonic) for supersonic retropropulsion phases with either full aerodynamic drag preservation or no aerodynamic drag preservation is significant. In the case of $\beta = 350$ kg/m^2, for full C_D preservation ($C_T = 1.0$), the total descent PMF would be nearly twice the supersonic PMF and, for no C_D preservation ($C_T = 3.0$), the total descent PMF would be nearly 3 times the supersonic PMF. Table 1 provides a summary of Fig. 1 in terms of supersonic descent propellant mass.

III. General Flow Characteristics

By the time aerodynamic drag has decelerated the vehicle to supersonic speeds, the vehicle is in the continuum flow regime where the Navier–Stokes equations are valid [38]. In this flow regime, the flow over a blunt entry vehicle is characterized by a strong detached bow shock [39]. Supersonic nozzle flow exhausting from a blunt body opposing a supersonic freestream results in an interaction between the nozzle flow and the detached bow shock. Flowfields surrounding blunt bodies with no retropropulsion, configurations with nozzle flow from the center of the vehicle forebody, and configurations with nozzle flow from the periphery of the vehicle forebody each exhibit fundamentally different behaviors. Flowfield geometry and stability are highly dependent on the nozzle location on the forebody (central vs peripheral) and the relative strength of the nozzle flow, often given as a function of the ratio of the total pressure of the jet flow to the total pressure of the freestream. For a fixed set of freestream conditions, characterized by the freestream total pressure, thrust coefficient is often used as a similarity parameter to gauge the strength of the nozzle flow relative to the freestream. As a result, the thrust coefficient is used as an independent parameter in the analysis when the freestream conditions are fixed.

A. Central Retropropulsion Configurations

The majority of the literature focuses on retropropulsion configurations in which either a single nozzle or a small cluster of nozzles is located along the forebody centerline. An example of a central retropropulsion configuration with a single nozzle is shown in Fig. 2.

Figure 3 (adapted from [13]) illustrates the characteristic flowfield features for a central retropropulsion configuration and the complexity of the interaction between the nozzle flow and the freestream shock structure. The primary flow structures are the bow shock, free stagnation point, jet terminal shock, and the recirculation regions. The location, degree of formation, and stability of these features are a strong function of the ratio of jet total pressure to freestream total pressure [13].

The supersonic retropropulsion flowfield structure is dependent on the formation of the free stagnation point. The freestream must decelerate to zero velocity, first from supersonic to subsonic through a shock wave, then from subsonic to zero velocity at the stagnation point [13]. The nozzle flow undergoes a similar deceleration through mixing, viscous dissipation, or a normal shock, depending on the

Table 1 Impact of aerodynamic-propulsive interactions on supersonic descent propellant mass with increasing ballistic coefficient

β, kg/m^2	Entry mass, kg	m_{prop}, kg (no aero)	m_{prop}, kg (with aero)	Difference, kg
150	34,459	1,616	772	844
200	45,946	3,951	1,916	1,990
250	57,432	8,144	4,003	4,141
300	68,919	13,549	6,774	6,775
350	80,405	19,659	9,954	9,705

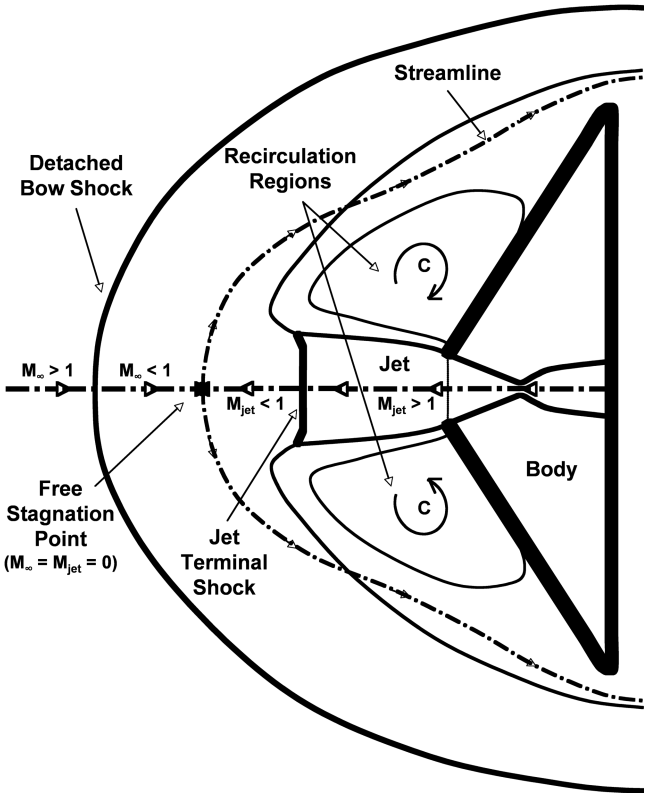

Fig. 3 Characteristic flowfield features for a central nozzle configuration (adapted from [13]).

degree of expansion of the nozzle exhaust flow. For supersonic retropropulsion, the stagnation region consists of two supersonic regions (the freestream and nozzle flow) and a subsonic region divided by a contact discontinuity (the stagnation point) [19].

The interaction of the nozzle exhaust with the opposing supersonic freestream for central retropropulsion configurations has been observed to cause the flowfield to transition from stable to highly unstable and back to stable as the total pressure ratio (or thrust coefficient) increases [13,14]. This behavior is illustrated by Mach number contours in Fig. 4 for a retropropulsion configuration with a single, centrally located nozzle [15]. A stable flowfield occurs when the bow shock is close to the body, and the nozzle exhaust flow does not penetrate the bow shock (Figs. 4a and 4c); in this case, the flowfield structure is not oscillating. An unstable flowfield (Fig. 4b) occurs when the nozzle exhaust flow penetrates the bow shock and the total shock displacement is significantly greater than the shock displacement characteristic of the stable condition (Fig. 4b vs Fig. 4c). This displacement increases to a maximum with increasing total pressure ratio and then collapses back to a displacement similar to the original stable case, illustrated through the progression in Fig. 4 [10,15,19].

This stability transition phenomenon is not thoroughly understood. However, the boundaries of the different flow regimes can be partially correlated to changes in relative mass flow and increases in the ratio of jet total pressure to freestream total pressure. At low flow rates (low total pressure ratios), the exhaust flow is retained within the shock layer and lacks sufficient momentum to disturb the bow shock [19].

As the nozzle flow rate increases, the nozzle flow cannot be contained within the shock layer and begins to interact with the bow shock. The shock standoff distance increases proportionally with increasing nozzle flow until reaching a maximum displacement on the order of 6–7 body diameters [14]. In this unstable regime, the dissipative mechanism that allows the jet total pressure to equal the freestream total pressure at the interface is viscosity. These viscous losses require a greater jet length for the pressure adjustment (i.e., flow deceleration) to occur [14].

As the flow rate increases further, the shock standoff distance begins to decrease, and the entire flow structure eventually collapses back to a stable condition. In this case, the primary dissipative mechanism is a terminal shock, with the resulting subsonic jet flow stable enough to form a distinct stagnation point [14,19]. The static pressure at the nozzle exit determines the expansion condition of the jet flow (under- or overexpanded), hence determining which of the dissipative mechanisms is likely dominant. Mixing and viscous dissipation are typically associated with underexpanded jet flow, and shock dissipation is common to overexpanded jet flow [14,40]. This transition from a stable to an unstable flowfield occurs at lower thrust coefficients for smaller nozzles and at larger thrust coefficients for larger nozzles, indicating a dependence on the ratio of the nozzle exit diameter to body diameter [16].

For a configuration of multiple nozzles arranged closely about the body's axis of symmetry, Peterson and McKenzie [17] observed the same stability transitions as seen for the single, centrally located nozzle. At low flow rates, the nozzle flows do not interact with one another. However, as the flow rate increases, the individual exhaust flows begin to coalesce and interact with the bow shock as a single jet flow, resulting in the large shock displacements characteristic of single-nozzle configurations.

B. Peripheral Retropropulsion Configurations

In contrast to the central retropropulsion configuration, few references are available on retropropulsion configurations with nozzles at the periphery of the forebody. The primary documented investigations on peripheral configurations are the experimental works by Jarvinen and Adams [10,11] and Keyes and Hefner [12]. In a peripheral retropropulsion configuration, such as the one shown in Fig. 5, the nozzle flow interacts with the bow shock differently than in a central configuration. Figure 6 illustrates the general flowfield for a peripheral retropropulsion configuration. The exhaust flow from each nozzle is swept away from the forebody and, at low flow rates, diffused into the opposing freestream by mixing [10]. Accordingly, flowfields for peripheral retropropulsion configurations do not have the large recirculation regions over the body surface characteristic of central configurations. Rather, the flowfield has a uniform region

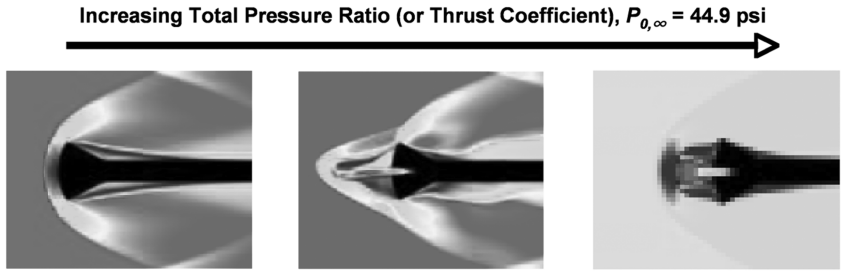

a) Stable flowfield $P_{o,jet}$ **= 0 psi**

b) Unstable flowfield $P_{o,jet}$ **= 133.4 psi**

c) Stable flowfield $P_{o,jet}$ **= 590.8 psi**

Fig. 4 Stability transitions with increasing jet flow for central configurations (CFD solutions [15]), $M_\infty = 3.48$.

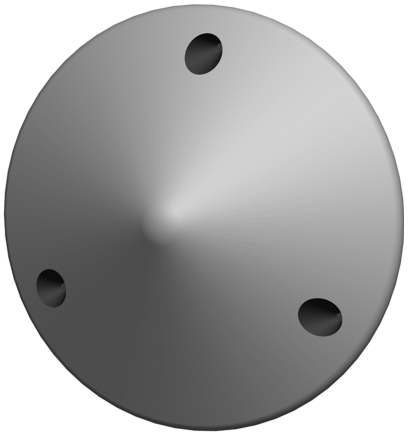

Fig. 5 Example of a peripheral retropropulsion configuration.

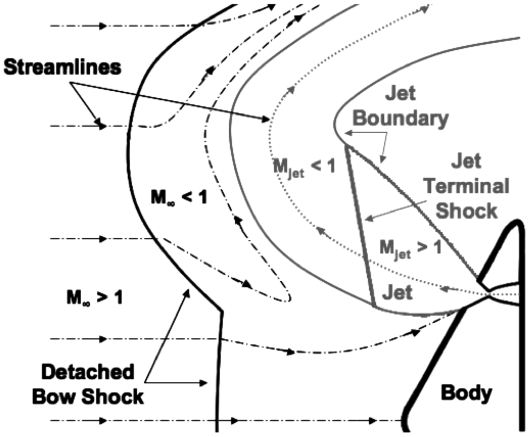

Fig. 6 Characteristic flowfield features of a peripheral nozzle configuration.

of high pressure inboard of the nozzles, resulting from the lack of disturbance to the portion of the bow shock nearest the nose of the blunt body. A smaller flow turning angle is required than for a central configuration, preventing the nozzle flow from disturbing the center of the bow shock.

As the thrust coefficient increases, the bow shock standoff distance increases. For larger values of C_T, the flowfield becomes increasingly unsteady as the jet flows begin to disturb the portion of the bow shock inboard of the nozzles. The nozzle flow now diffuses through a terminal shock instead of mixing with the freestream [10]. Both Jarvinen and Adams [10,11] and Keyes and Hefner [12] observed local instabilities affecting the slope of the bow shock as the total thrust coefficient increased beyond $\sim$3. However, the sharp increase in standoff distance and dissolution of the bow shock characteristic of the central retropropulsion configuration have not been observed with the peripheral configuration. Future experimental and computational work will be required to fully characterize the flowfield stability of configurations with peripheral nozzles.

IV. Aerodynamic Characteristics and Experimental Data Summary

The effects of supersonic retropropulsion on the aerodynamics of blunt body entry vehicles influence the retropropulsion configurations desirable for EDL supersonic deceleration. The forebody nozzle configuration (i.e., central vs peripheral) and the ratio of the jet total pressure to the freestream total pressure govern the aerodynamic forces and static stability. Central and peripheral retropropulsion configurations exhibit fundamentally different flow behavior, resulting in contrasting aerodynamic effects.

A. Aerodynamic Characteristics

1. Central Retropropulsion Configurations

A substantial number of experiments were performed from the late 1950s through the early 1970s on the aerodynamic effects of a centrally located retronozzle for EDL applications. These experiments used blunt cones, hemispheres, and other bodies of revolution at Mach numbers from 1.05 to 9. With increasing thrust coefficient, the aerodynamic drag coefficient decreases rapidly to a minimum value of approximately 10% of the no-jet value and then remains constant at this minimum value. For thrust coefficients above approximately 0.4, the total axial force coefficient is dominated by the contribution from thrust. Above $C_T \sim 0.8$, the increment of $C_{A,\text{total}}$ above C_T is roughly constant, with this increment due to the minimally preserved aerodynamic drag coefficient. These effects are shown in Fig. 7 (adapted from [16]).

With flow from a central nozzle, the high inboard pressure present in the no-jet case is greatly reduced. The nozzle flow perturbs the bow shock to become more oblique than normal. This reduction in shock strength leads to a reduction in surface pressure and, thus, aerodynamic drag [18]. The degree of this surface pressure reduction tends to increase as the freestream Mach number increases [16].

At thrust coefficients greater than approximately 0.2, the nozzle flow cannot be contained within the boundary layer, and a sharp flow turning angle causes the boundary layer to separate on both sides of the jet on the forebody. Strong recirculation regions form on both sides of the nozzle flow, moving the flow within the shock layer toward the vehicle shoulder. Flow reattachment begins near a thrust coefficient of 2 and, by higher thrust coefficients (at $C_T \sim 6$), the body base pressure equals the forebody pressure, enveloping the body in a constant pressure region similar to wake flow [10,16]. Little variation in the surface pressure is seen between different blunt body geometries, indicating a relative independence of aeroshell cone angle on the drag reduction effects of central retropropulsion configurations.

Romeo and Sterrett [14] examined flowfield stability for a centrally located nozzle over angles of attack from 0 to 35 deg. Beyond very small angles of attack (greater than 2 deg), the structure of the flowfield breaks down for total pressure ratios (or thrust coefficients) corresponding to cases in which the nozzle exhaust flow penetrates the bow shock, resulting in a large standoff distance.

The pitching moment coefficient slopes for increasing thrust coefficients at freestream Mach numbers of 0.6, 1.05, and 2.0 are shown in Fig. 8 [10]. The pitching moment is referenced from the apex of the aeroshell cone. The data were taken over angles of attack from -6 to $+6$ deg. For the central nozzle configuration, the pitching moment coefficient slope for a given thrust coefficient is nearly linear with variation in angle of attack across the range tested

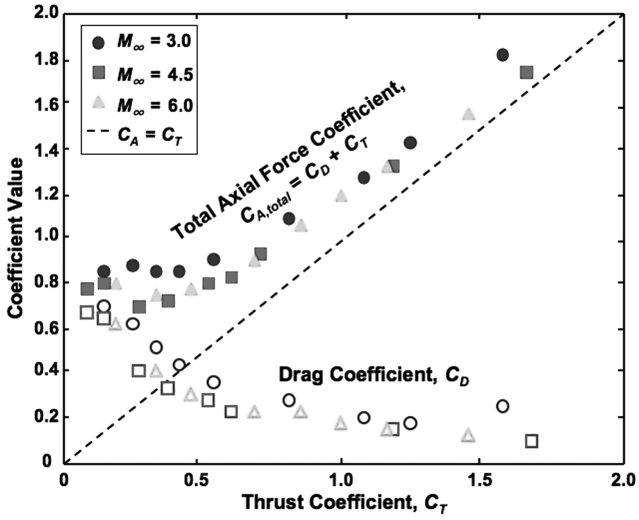

Fig. 7 Aerodynamic drag coefficient variation with increasing thrust coefficient for central nozzle location (adapted from [16]).

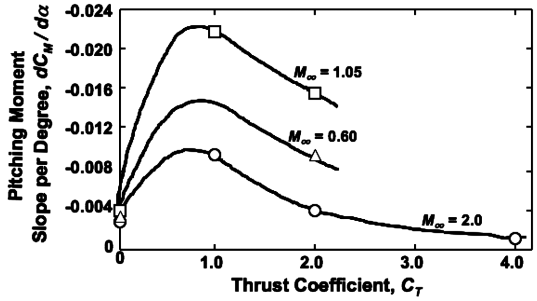

Fig. 8 Variation of pitching moment slope with thrust coefficient [10].

(−6– + 6 deg), resulting in data for a specific angle of attack not distinguished in Fig. 8. The pitching moment coefficient slope becomes increasingly negative as the thrust coefficient increases to 1, then becomes less negative with additional increases in thrust coefficient. The pitching moment coefficient slope is always negative, indicating static stability about the reference point across the range of thrust coefficients tested. This static stability is observed even in cases in which the flowfield itself may be unstable.

2. *Peripheral Retropropulsion Configurations*

Experimental data have been taken at freestream Mach numbers of 1.05, 1.50, 2.0, and 6.0, using 60 deg sphere cones and air for the freestream and nozzle flow [10–12]. Jarvinen and Adams [10,11] and Keyes and Hefner [12] observed a lack of disruption of the center of the bow shock by the peripheral nozzle flow. The nozzle flow being swept away from the vehicle causes a region of high pressure to remain over portions of the aeroshell inboard of the nozzles, preserving the aerodynamic drag [10–12], as illustrated previously in Fig. 6. The bow shock remains sufficiently undisturbed and close to the body for total thrust coefficients below ∼2 [10].

Experimental work by Jarvinen and Adams [10,11] demonstrated a range of thrust coefficients over which a three-nozzle peripheral configuration (see Fig. 5) resulted in a substantially larger total axial force coefficient than a single, centrally located nozzle at the same total thrust coefficient. A comparison of the total axial force coefficient between a peripheral nozzle configuration and a central nozzle configuration at the same conditions is shown in Fig. 9 [10].

A retropropulsion configuration with three nozzles at the body periphery is more aerodynamically efficient than the configuration with a single central nozzle for thrust coefficients up to ∼2. At thrust coefficients above ∼3, the total axial force coefficients for both configurations are nearly equal to the thrust coefficient alone, shown by the dashed line in Fig. 9 [10]. At lower thrust coefficients, the peripheral nozzle flow only mildly disturbs the bow shock at the edges. This perturbation flattens the bow shock at the edges, causing the flowfield to see the entire blunt body. At higher thrust coefficients, the peripheral nozzle flow penetrates the bow shock, and the high-pressure region inboard of the nozzles disappears as the bow shock weakens [10,12].

The augmentation of the total axial force coefficient by drag preservation is dependent on freestream Mach number. The maximum degree of aerodynamic drag preservation, observed near a thrust coefficient of 1, increases over the freestream Mach numbers tested, likely due to the increasing strength of the bow shock [10]. In these cases, an axial force augmentation from aerodynamics approximately equal to the thrust force is possible. Surface pressure data confirm that the aeroshell is influenced by a nearly uniform region of high pressure, and this surface pressure is highest at total thrust coefficients near 1 [10].

Variation in angle of attack, from −6 to +6 deg, causes little effect on the total forebody axial force coefficient for freestream Mach numbers of 1.05, 1.50, and 2.0 with thrust coefficients from 0 to 1.9 [10]. However, the pitching moment coefficient exhibits nonlinear behavior at Mach 2, as shown in Fig. 10 [10]. As in the central nozzle case, the pitching moment coefficient is referenced from the apex of the aeroshell cone. For a thrust coefficient of 1.04, the pitching moment coefficient slope is positive for angles of attack between −2 and −8 deg. With the limited data available for this configuration, the nonlinearity and indiscernible dependence on thrust coefficient cause difficulty in determining the relationship between static stability about this reference point and C_T.

3. *Differential Throttling Effects*

Jarvinen and Adams [10,11] also explored potential drag modulation capability by throttling various combinations of three engines in a peripheral configuration. The variation in total axial force coefficient between the throttled and unthrottled conditions was observed to increase with increasing freestream Mach number. At a freestream Mach number of 1.05, little variation between the unthrottled case and the cases in which one engine was throttled down by either 50 or 75% was observed for thrust coefficients below ∼3. However, in a Mach 2.0 freestream, significant variation between the two cases (unthrottled vs throttled down) was observed at total thrust coefficients above ∼1.

Similar departures were observed under the same conditions for cases in which two of the three engines were throttled down [10]. In the $M_\infty = 1.05$ case, with one engine throttled down by 50% and the total thrust coefficient increased from 0.5 to 3.0, the forebody drag coefficient decreased from 0.8 to approximately 0. At the same freestream conditions, with two engines throttled down and the thrust coefficient increased from 0.5 to 3.0, the forebody drag coefficient

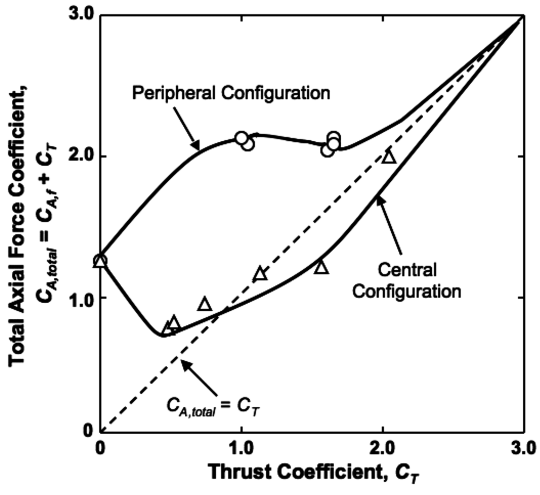

Fig. 9 Comparison of total axial force coefficient for peripheral and central configurations, $M_\infty = 2.0$ [10].

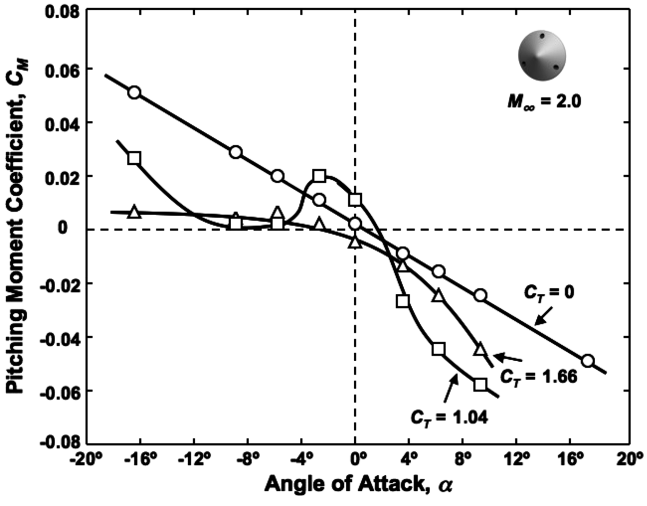

Fig. 10 Variation of pitching moment coefficient with thrust coefficient and angle of attack [10].

decreased from 0.8 to approximately −0.4. At higher thrust coefficients, the disruption of the bow shock by the asymmetric jet flow resulted in surface pressure measurements lower than the freestream static pressure; thus, negative force coefficients were possible at these conditions. In the $M_\infty = 2.0$ case, with one engine throttled down and the thrust coefficient increased from 0.5 to 3.0, the forebody drag coefficient decreased from 1.2 to approximately −0.1. In the $M_\infty = 2.0$ case, with two engines throttled down and the thrust coefficient increased from 0.5 to 3.0, the forebody drag coefficient decreased from 1.2 to approximately 0.1. Jarvinen and Adams [10] concluded that, as freestream Mach number increased, the same degree of forebody drag coefficient modulation could be realized with decreasing thrust coefficients.

Throttling various combinations of engines at the body periphery alters the static stability of the vehicle [10]. The total pitching moment on the body is the sum of the pitching moment due to surface pressure forces and the pitching moment induced by imbalances in thrust. In cases in which the body is oriented at a positive angle of attack, throttling down engines on the leeward side of the forebody induces a nose-down pitching moment. In the same orientation, throttling down engines on the windward side of the forebody induces a nose-up pitching moment [10].

These induced pitching moments can be attributed to the asymmetry of the bow shock, a condition arising from the nonuniform engine thrust and resulting total axial force changes at throttled conditions. Schlieren images [10] show an increase in standoff distance and an increase in the obliqueness of the local section of the bow shock in the region of the unthrottled nozzle flow. The decrease in shock strength with the increase in obliqueness supports the conclusion that the reduction in the total axial force coefficient with increasing thrust coefficient (as compared with the unthrottled case) is strongly dependent on changes to the surface pressure distribution caused by throttling. The effectiveness of throttling in controlling pitching moment, defined as the ratio of change in pitching moment measured experimentally to the change in pitching moment due solely to an imbalance in engine thrust, is observed to be reduced by 20% at supersonic freestream conditions as compared with throttling efficiency at subsonic velocities [10]. Jarvinen and Adams [10,11] attributed this reduction in throttling effectiveness to the effect of supersonic freestream conditions on the total axial force coefficient.

B. Experimental Summary

The focused technology development program for planetary exploration missions in the 1960s and early 1970s matured supersonic retropropulsion close to its current level of readiness through a number of experimental investigations. The intent of these experiments was to understand drag effects potentially advantageous to EDL. Scaling parameters were developed to accurately simulate the larger chemical bipropellant propulsion systems visualized for conceptual Mars landers using subscale models [30]. The freestream Mach number, thrust coefficient, plume sensitivity parameter, and engine scaling parameter are the parameters to be matched for proper simulation of retrorocket flow at subscale in a wind tunnel [10,30]. No supersonic retropropulsion aerodynamic data have been found in support of missions to destinations other than Mars.

Although numerous wind-tunnel tests have been conducted, the scope of the work was limited in the freestream conditions, retropropulsion conditions, and body geometries explored. The majority of past efforts focused on blunt bodies with a single, centrally located nozzle. Only three investigations have been found that used multiple nozzles [10–12,17]. An additional limitation of the existing data is the use of compressed air, nitrogen, hydrogen, or helium in all test cases for the nozzle exhaust. No experimental data exist in which combustion products were exhausted, possibly due to test scale and the complexity of combustion systems. In addition, the primary goal of many investigations was to explore potential reductions in heat transfer, not decelerator performance. The flow conditions and geometries that make up the existing experimental database are summarized in Table 2. The maximum model size used in any of these experiments was 8.25 in. (model diameter).

This experimental database will need to be expanded to include additional retropropulsion configurations, body geometries, exhaust and freestream species, combustion retropropulsion systems, and a broader range of flow conditions. Additionally, slender body geometries such as biconics and ellipsleds are candidates for human Mars architectures, and no data exist to validate computational simulation of supersonic retropropulsion systems derived for these geometries. As the work by Peterson and McKenzie [17] is the only configuration of multiple nozzles not located on the body periphery, performance trends for the required nozzle spacing to prevent an interaction between exhaust jets are also unknown.

V. Computational Analyses in the Literature

The complexity of supersonic retropropulsion interactions challenges the computational simulation of these coupled flowfields, particularly in starting solutions, defining convergence, handling oscillatory behavior, and matching surface pressure and heat transfer distributions. Few papers have been published on the computational modeling and analysis of supersonic retropropulsion [15,23,28,31,32,45,46]. Most of the work focuses on the mitigation of severe aerothermal environments during entry, drag reduction for entry vehicles, and plasma interactions for controlling shock strength in supersonic freestreams [23,28,45,46]. However, the similarities between the aerodynamic-propulsive interactions

Table 2 Existing supersonic retropropulsion experimental database

Available central nozzle configuration data				
Relevance	Freestream Mach	Freestream	Jet	References
Static aerodynamics	1.05–6.0, 20–21	Air	Air, helium	[10,11,13–26,31,41–44]
Flowfield stability	1.05–6.0	Air	Air, helium	[10,11,13,16–18,23]
Flowfield geometry	1.05–8.0	Air	Air, helium	[10,11,13–17,19–21,25,41–44]
Effect of nozzle geometry	1.05–6.0, 20–21	Air	Air, helium	[10,11,13–15,24,26,42]
Angle of attack variation	1.05–6.0	Air	Air, helium	[10,11,14,16,17]
Aerothermodynamics	2.0, 6.0–8.0, 20–21	Air	Air, helium, nitrogen, hydrogen	[15,19,21–29,32]
Systems-level implications	1.05–6.0	Air	Air	[10,11,14,18,26]
Available peripheral nozzle configuration data				
Relevance	Freestream Mach	Freestream	Jet	References
Static aerodynamics	1.05–6.0	Air	Air	[10–12]
Flowfield stability	1.05–2.0	Air	Air	[10,11]
Flowfield geometry	1.05–2.0	Air	Air	[10–12]
Effect of nozzle geometry	1.05–2.0	Air	Air	[10,11]
Angle of attack variation	1.05–2.0	Air	Air	[10,11]
Aerothermodynamics	——	——	——	——
Systems-level implications	1.05–2.0	Air	Air	[10–12]

across these works have been useful in extending existing computational approaches to analyses targeting drag preservation and augmentation applications for high-mass entry systems.

Computational solutions for supersonic retropropulsion systems should capture the following characteristics: 1) flow features such as detached shocks, shock/boundary-layer interactions, shock–shock interactions, and recirculation; 2) viscous effects within the shock layer; 3) jet flow expansion; and 4) relevant equilibrium chemistry.

Several recent studies [15,23,28,31,32,45,46] have shown some success in modeling the aerodynamics and aerothermodynamics of single-nozzle configurations.

Daso et al. [15] conducted computational fluid dynamics (CFD) analyses with a 2.6%-scale Apollo capsule with and without retropropulsion effects in support of a recent test series. An additional posttest study was completed by Cheng et al. [31] and Chang et al. [32]. In all cases, the CFD analyses were attempting to predict the aerodynamic and aerothermodynamic effects of a centrally located nozzle in air at freestream Mach numbers of 3.48 and 4.0. Both the computational simulations and associated experiment used compressed air for the nozzle exhaust [15]. The use of time-accurate Navier–Stokes solvers predicted the transitions in flow stability and captured the general aerothermodynamic trends observed in subsequent testing, whereas the steady-state solutions were less successful in matching experimental results for cases with significant jet–shock interaction. The characteristic unsteadiness and oscillatory behavior of the flowfields with retropropulsion were observed in all cases. Time histories of aerodynamic drag and surface heat flux quantities exhibited low-frequency, large-amplitude oscillations. In general, the analyses show relatively good agreement with the experimental data with tendencies to underpredict pressure and overpredict heat flux.

Fomin et al. [45] performed numerical simulations in support of experimental work on the blunt body pressure effects of a centrally located, high-temperature plasma jet at freestream Mach numbers of 2.0, 2.5, and 4.0. The composition of the freestream was air, and the plasma jet was nitrogen gas at 5000 K. Experimental results were compared against an Euler CFD analysis in an effort to understand the separation existing between fluid dynamics and the thermal processes in a supersonic freestream-propulsion interaction. An Euler solver was able to capture the reduction in body surface pressures caused by the transition to unstable flow and jet penetration of the bow shock. The relatively good pressure distribution agreement seen between the Euler solutions and the experimental plasma jet work suggests that much of the interactions at supersonic Mach numbers resemble retropropulsion gas dynamics, a promising result for future work focused on the inclusion of combustion products [45]. Additional work [46] has been reported in which the plasma jets are modeled using the assumption of a perfect gas with constant specific heats.

Hayashi et al. [23] solved the axisymmetric Navier–Stokes equations to predict reductions in aerothermal heating in the stagnation region of a hemisphere at a freestream Mach number of 3.96. The freestream composition was air, and the nozzle exhaust was nitrogen gas at 300 K. The CFD results showed good agreement with the experiment, particularly in the ability to capture the recirculation regions about a centrally located jet. The strength of the recirculation regions was slightly higher than observed experimentally, resulting in a larger heat flux reduction in the CFD solution than observed in the experiment.

Computational simulation of the interactions between retropropulsion exhaust flows and supersonic freestreams is the next phase of investigation required to mature supersonic retropropulsion from a potentially feasible concept to an applicable EDL technology. Much of the physics relevant to the flowfield behavior is coupled and viscous in nature. Flow separation, recirculation, boundary-layer transition, and oscillation of the primary flow features such as the detached bow shock, free stagnation point, and jet flow boundary are relevant characteristics of supersonic retropropulsion flowfields. Computational solutions that accurately capture these characteristics exist under a very limited range of conditions at this point.

VI. Conclusions

Interactions between retropropulsion exhaust and blunt body aerodynamics have been investigated since the early 1950s. Extensive wind-tunnel experiments in the 1960s and early 1970s developed the technology to near the level of maturity it has today. Experimental results consistently show significant benefit (preservation of aerodynamic drag) for peripheral retropropulsion configurations at low thrust coefficients. The literature also demonstrates little or no axial force augmentation beyond that provided by the retropropulsive thrust for configurations with the nozzle located along the body centerline. The degree of aerodynamic interaction is strongly dependent on the location of the nozzles and the relative strength of the exhaust flow to the freestream. The primary parameter used to characterize the static aerodynamics and flowfield stability is the thrust coefficient, with the greatest degree of axial force augmentation for peripheral retropropulsion configurations occurring near a thrust coefficient of 1.

The severe reduction in aerodynamic drag for central retropropulsion configurations is a drawback to this technology's application to supersonic deceleration. The flowfield stability transitions and observed flow unsteadiness over most freestream Mach numbers and thrust coefficients investigated are additional complications to the implementation of this configuration into an EDL architecture.

The marked increase in the total axial force coefficient for low-to-modest thrust coefficients makes peripheral retropropulsion configurations favorable for application as a supersonic decelerator. The maximum augmentation in total axial force occurs at conditions typical of stable flowfields. However, the existing experimental database for peripheral configurations is limited, suggesting a need to expand the database to additional configurations and conditions for accurate comparison with alternative supersonic decelerator technologies.

The most significant challenges in maturing supersonic retropropulsion are related to a lack of knowledge in the following areas: 1) configurations with nozzles at the body periphery, 2) aerodynamic interactions on slender body vehicle geometries, 3) aerothermal effects caused by exhausting combustion products into the shock layer, 4) uncertainties in scaling wind-tunnel results to flight systems, and 5) validated computational fluid dynamics approaches.

References

[1] Braun, R. D., and Manning, R. M., "Mars Exploration Entry, Descent, and Landing Challenges," *Journal of Spacecraft and Rockets*, Vol. 44, No. 2, 2007, pp. 310–323. doi:10.2514/1.25116

[2] Love, E. S., "The Effect of a Small Jet of Air Exhausting from the Nose of a Body of Revolution in Supersonic Flow," NACA RM L52I19a, Nov. 1952.

[3] Love, E. S., "A Re-Examination of the Use of Simple Concepts for Predicting the Shape and Location of Detached Shock Waves," NACA TN-4170, 1957.

[4] Love, E. S., Grigsby, C. E., Lee, L. P., and Woodling, M. J., "Experimental and Theoretical Studies of Axisymmetric Free Jets," NASA TR R-6, 1959.

[5] Huff, R. G., and Abdalla, K. L., "Mixing Characteristics Downstream of Core Region of High-Temperature Axisymmetric Jets Exhausting into Transonic and Supersonic Streams," NASA TM X-151, March 1960.

[6] Moeckel, W. E., "Flow Separation Ahead of Blunt Bodies at Supersonic Speeds," NACA TN 2418, July 1951.

[7] Moeckel, W. E., "Flow Separation Ahead of a Blunt Axially Symmetric Body at Mach Numbers 1.76 to 2.10," NACA RM E51I25, Dec. 1951.

[8] Love, E. S., Woodling, M. J., and Lee, L. P., "Boundaries of Supersonic Axisymmetric Free Jets," NACA RM L56G18, Oct. 1956.

[9] Love, E. S., and Grigsby, C. E., "Some Studies of Axisymmetric Free Jets Exhausting From Sonic and Supersonic Nozzles into Still Air and into Supersonic Freestreams," NACA RM L54L31, May 1955.

[10] Jarvinen, P. O., and Adams, R. H., "The Aerodynamic Characteristics of Large Angled Cones with Retrorockets," NASA CR NAS 7-576, Feb. 1970.

[11] Jarvinen, P. O., and Adams, R. H., "The Effects of Retrorockets on the Aerodynamic Characteristics of Conical Aeroshell Planetary Entry Vehicles," AIAA Paper 70-219, Jan. 1970.

[12] Keyes, J. W., and Hefner, J. N., "Effect of Forward Facing Jets on Aerodynamic Characteristics of Blunt Configurations at Mach 6," *Journal of Spacecraft and Rockets*, Vol. 4, No. 4, 1967, pp. 533–534. doi:10.2514/3.28900

[13] Finley, P. J., "The Flow of a Jet from a Body Opposing a Supersonic Free Stream," *Journal of Fluid Mechanics*, Vol. 26, No. 2, 1966, pp. 337–368. doi:10.1017/S0022112066001277

[14] Romeo, D. J., and Sterrett, J. R., "Exploratory Investigation of the Effect of a Forward-Facing Jet on the Bow Shock of a Blunt Body in a Mach Number 6 Free Stream," NASA TN D-1605, Feb. 1963.

[15] Daso, E. O., Pritchett, V. E., and Wang, T. S., "The Dynamics of Shock Dispersion and Interactions in Supersonic Freestreams with Counterflowing Jets," AIAA Paper 2007-1423, Jan. 2007.

[16] McGhee, R. J., "Effects of a Retronozzle Located at the Apex of a 140° Blunt Cone at Mach Numbers of 3.00, 4.50, and 6.00," NASA TN D-6002, Jan. 1971.

[17] Peterson, V. L., and McKenzie, R. L., "Effects of Simulated Retrorockets on the Aerodynamic Characteristics of a Body of Revolution at Mach Numbers from 0.25 to 1.90," NASA TN D-1300, May 1962.

[18] Charczenko, N., and Hennessey, K. W., "Investigation of a Retrorocket Exhausting from the Nose of a Blunt Body into a Supersonic Free Stream," NASA TN D-751, Sept. 1961.

[19] Barber, E. A., "An Experimental Investigation of Stagnation-Point Injection," *Journal of Spacecraft and Rockets*, Vol. 2., No. 5, 1965, pp. 770–774. doi:10.2514/3.28277

[20] Romeo, D. J., and Sterrett, J. R., "Flow Field for Sonic Jet Exhausting Counter to a Hypersonic Mainstream," *AIAA Journal*, Vol. 3, No. 3, 1965, pp. 544–546. doi:10.2514/3.2907

[21] Barber, E. A., "An Experimental Investigation of Stagnation-Point Injection," AIAA Paper 1963-0433, Aug. 1963.

[22] Warren, C. H. E., "An Experimental Investigation of the Effect of Ejecting a Coolant Gas at the Nose of a Bluff Body," *Journal of Fluid Mechanics*, Vol. 8, No. 3, 1960, pp. 400–417. doi:10.1017/S0022112060000694

[23] Hayashi, K., Aso, S., and Tani, Y., "Numerical Study of Thermal Protection System by Opposing Jet," AIAA Paper 2005-0188, Jan. 2005.

[24] Stalder, J. R., and Inouye, M., "A Method of Reducing Heat Transfer to Blunt Bodies by Air Injection," NACA RM A56B27a, May 1956.

[25] Grimaud, J. E., and McRee, L. C., "Experimental Data on Stagnation-Point Gas Injection Cooling on a Hemisphere-Cone in a Hypersonic Arc Tunnel," NASA TM X-983, July 1964.

[26] Grenich, A. F., and Woods, W. C., "Flow Field Investigation of Atmospheric Braking for High Drag Vehicles with Forward Facing Jets," AIAA Paper 1981-0293, Jan. 1981.

[27] Roberts, L., "Mass Transfer Cooling Near the Stagnation Point," NASA TR R-8, 1959.

[28] Hayashi, K., and Aso, S., "Effect of Pressure Ratio on Aerodynamic Heating Reduction due to Opposing Jet," AIAA Paper 2003-4041, June 2003.

[29] Chung, P. M., "Effect of Localized Mass Transfer Near the Stagnation Region of Blunt Bodies in Hypersonic Flight," NASA TN D-141, May 1960.

[30] Pindzola, M., *Jet Simulation in Ground Test Facilities*, AGARDograph 79, AGARD, Paris, Nov. 1963.

[31] Cheng, G. C., Neroorkar, K. D., Chen, Y-S, Wang, T-S, and Daso, E. O., "Numerical Study of Flow Augmented Thermal Management for Entry and Re-Entry Environments," AIAA Paper 2007-4560, June 2007.

[32] Chang, C-L., Venkatachari, B. S., and Cheng, G. C., "Effect of Counterflow Jet on a Supersonic Reentry Capsule," AIAA Paper 2006-4776, July 2006.

[33] Drake, B. G., "Reference Mission Version 3.0: Addendum to the Human Exploration of Mars: The Reference Mission of the NASA Mars Exploration Study Team," NASA SP-6107-ADD, June 1998.

[34] Hoffman, S. J., and Kaplan, D. I., "Human Exploration of Mars: The Reference Mission of the NASA Mars Exploration Study Team," NASA Johnson Space Center Rept. SP 6107, July 1997.

[35] Christian, J. A., Wells, G. W., Lafleur, J. M., Verges, A. M., and Braun, R. D., "Extension of Traditional Entry, Descent, and Landing Technologies for Human Mars Exploration," *Journal of Spacecraft and Rockets*, Vol. 45, No. 1, 2008, pp. 130–141. doi:10.2514/1.31929

[36] Wells, G. W., Lafleur, J. M., Verges, A. M., Manyapu, K., Christian, J. A., Lewis, C., and Braun, R. D., "Entry, Descent, and Landing Challenges of Human Mars Exploration," American Astronautical Society Paper 06-072, Feb. 2006.

[37] Tanner, L. G., "Development and Characteristics of the Russian/American RD-180 Rocket Engine," *AIAA Joint Propulsion Conference —Liquid Propulsion Short Course*, AIAA, Reston, VA, July 2002, pp. 1–26.

[38] Gnoffo, P. A., "Planetary-Entry Gas Dynamics," *Annual Review of Fluid Mechanics*, Vol. 31, 1999, pp. 459–494. doi:10.1146/annurev.fluid.31.1.459

[39] Campbell, J. F., "Supersonic Aerodynamic Characteristics and Shock Standoff Distances for Large-Angle Cones with and Without Cylindrical Afterbodies," NASA TN D-5334, Aug. 1969.

[40] Watt, G. A., "An Experimental Investigation of a Sonic Jet Directed Upstream Against a Uniform Supersonic Flow," Inst. of Aerophysics, Univ. of Toronto TN 7, Jan. 1956.

[41] Margason, R. J., "The Path of a Jet Directed at Large Angles to a Subsonic Free Stream," NASA TN D-4919, Nov. 1968.

[42] Jarvinen, P. O., and Hill, J. A. F., "Penetration of Retrorocket Exhausts into Subsonic Counterflows," *Journal of Spacecraft and Rockets*, Vol. 10, No. 1, 1973, pp. 85–86. doi:10.2514/3.27737

[43] Hayman, L. O., and McDearmon, R. W., "Jet Effects on Cylindrical Afterbodies Housing Sonic and Supersonic Nozzles which Exhaust against a Supersonic Stream at Angles from 90 to 180 Degrees," NASA TN D-1016, March 1962.

[44] Baron, J. R., and Alzner, E. R., "An Experimental Investigation of a Two Layer Inviscid Shock Cap Due to Blunt Body Nose Injection," *Journal of Fluid Mechanics*, Vol. 15, No. 3, 1963, pp. 442–448. doi:10.1017/S0022112063000367

[45] Fomin, V. M., Maslov, A. A., and Malmuth, N. D., "Influence of a Counterflow Plasma Jet on Supersonic Blunt-Body Pressures," *AIAA Journal*, Vol. 40, No. 6, 2002, pp. 1170–1177. doi:10.2514/2.1768

[46] Chernyi, G. G., "Some Recent Results in Aerodynamic Applications of Flows with Localized Energy Addition," AIAA Paper 99-4819, Nov. 1999.

R. Cummings
Associate Editor